Curved focal plane extreme ultraviolet detector array for a EUV camera on CHANG E lander

Q. Ni,[1,*] K. Song,[1] S. Liu, [1]L. He,[1] B. Chen,[1] and W. Yu[2,3]

[1]*Changchun Institute of Optics, Fine mechanics and Physics, Chinese Academy of Sciences, 3888 Dongnanhu Road, Changchun, China*

[2]*Insititue of Micro and Nano Optics, Key Laboratory of Optoelectronic Devices and Systems of Ministry of Education and Guangdong Province, College of Optoelectronic Engineering, Shenzhen University, Shenzhen 518060, China*

[3]*yuwx@szu.edu.cn*

[*]*niqiliang@hotmail.com*

Abstract: A novel curved focal plane extreme ultraviolet (EUV) detector array designed for a moon-based EUV camera is demonstrated. The curved focal plane detector array operating in a pulse-counting mode consists of a curved microchannel plate (MCP) stack and an induced charge wedge-strip anode (WSA). The curved MCP is fabricated by firstly thermally slumping of the MCPs, and then followed by optical polishing and core glass etching. By using this technology, curved MCPs with a length-to-diameter (L/D) ratio of 80:1 and a radius of curvature of 150 mm have been successfully achieved. The performance of the curved MCP detector is fully characterized in terms of the background noise, pulse height distribution, gain, image linearity and spatial resolution. It is measured that a spatial resolution of 7.13 lp/mm can be achieved with a background noise of less than 0.3 counts/cm^2·s. The characterization results indicate that the curved focal plane detector can fulfill the requirements of the moon-based EUV camera.

OCIS codes: (040.1240) Arrays; (040.5160) Photodetectors; (040.5250) Photomultipliers; (040.7480) X-rays, soft x-rays, extreme ultraviolet (EUV).

References and links

1. S.-B. Rim, P. B. Catrysse, R. Dinyari, K. Huang, and P. Peumans, "The optical advantages of curved focal plane arrays," Opt. Express **16**(7), 4965–4971 (2008).
2. H. Jin, J. R. Abelson, M. K. Erhardt, and R. G. Nuzzo, "Soft lithographic fabrication of an image sensor array on a curved substrate," J. Vac. Sci. Technol. B **22**(5), 2548–2551 (2004).
3. P. J. Hung, K. Jeong, G. L. Liu, and L. P. Lee, "Microfabricated suspensions for electrical connections on the tunable elastomer membrane," Appl. Phys. Lett. **85**(24), 6051–6053 (2004).
4. H. C. Ko, M. P. Stoykovich, J. Song, V. Malyarchuk, W. M. Choi, C. J. Yu, J. B. Geddes 3rd, J. Xiao, S. Wang, Y. Huang, and J. A. Rogers, "A hemispherical electronic eye camera based on compressible silicon optoelectronics," Nature **454**(7205), 748–753 (2008).
5. R. Dinyari, S.-B. Rim, K. Huang, P. B. Catrysse, and P. Peumans, "Curving monolithic silicon for nonplanar focal plane array applications," Appl. Phys. Lett. **92**, 191114 (2008).
6. X. Xu, M. Davanco, X. F. Qi, and S. R. Forrest, "Direct transfer patterning on three dimensionally deformed surfaces at micrometer resolutions and its application to hemispherical focal plane detector arrays," Org. Electron. **9**(6), 1122–1127 (2008).
7. I. Jung, J. Xiao, V. Malyarchuk, C. Lu, M. Li, Z. Liu, J. Yoon, Y. Huang, and J. A. Rogers, "Dynamically tunable hemispherical electronic eye camera system with adjustable zoom capability," Proc. Natl. Acad. Sci. U.S.A. **108**(5), 1788–1793 (2011).
8. D. Dumas, M. Fendler, N. Baier, J. Primot, and E. le Coarer, "Curved focal plane detector array for wide field cameras," Appl. Opt. **51**(22), 5419–5424 (2012).
9. Y. M. Song, Y. Xie, V. Malyarchuk, J. Xiao, I. Jung, K.-J. Choi, Z. Liu, H. Park, C. Lu, R.-H. Kim, R. Li, K. B. Crozier, Y. Huang, and J. A. Rogers, "Digital cameras with designs inspired by the arthropod eye," Nature **497**(7447), 95–99 (2013).
10. B. R. Sandel, A. L. Broadfoot, C. C. Curtis, R. A. King, T. C. Stone, R. H. Hill, J. Chen, O. H. W. Siegmund, R. Raffanti, D. D. Allred, R. S. Turley, and D. L. Gallagher, "The extreme ultraviolet imager investigation for the image mission," Space Sci. Rev. **91**(1/2), 197–242 (2000).

#242423 Received 5 Jun 2015; revised 1 Nov 2015; accepted 10 Nov 2015; published 17 Nov 2015

11. J. J. Bloch, B. C. Edwards, W. C. Priedhorsky, D. C. Roussel-Dupre, B. W. Smith, O. H. W. Siegmund, T. Carone, S. L. Cully, T. Rodriguez-Bell, J. K. Warren, and J. V. Vallerga, "On orbit performance of the ALEXIS EUV telescopes," Proc. SPIE **2280**, 297–309 (1994).
12. C. Martin, P. Jelinsky, M. Lampton, and R. F. Malina, "Wedge-and-strip anodes for centroid-finding position-sensitive photon and particle detectors," Rev. Sci. Instrum. **52**(7), 1067–1074 (1981).
13. S. Nikzad, M. Hoenk, and T. A. Jones, "Solid-state curved focal plane arrays," United States Patent Application, 20050109918, (May 26, 2005) 250/208.1.
14. T. J. Jones and S. Nikzad, "Curved focal plane arrays using conformed thinned detector membrane," Nanotech Briefs **28**, 3 (2004).
15. R. Dinyari, S.-B. Rim, K. Huang, P. B. Catrysse, and P. Peumans, "Curving monolithic silicon for non-planar focal plane array applications," Appl. Phys. Lett. **92**(9), 091114 (2008).
16. S. A. Stern, D. C. Slater, J. Scherrer, J. Stone, M. Versteeg, M. F. Ahearn, J. L. Bertaux, P. D. Feldman, M. C. Festou, J. W. Parker, and O. H. W. Siegmund, "Alice: the Rosetta Ultraviolet Imaging Spectrograph," Space Sci. Rev. **128**(1-4), 507–527 (2007).
17. O. H. W. Siegmund, M. A. Gummin, J. M. Stock, G. Naletto, G. A. Gaines, R. Raffanti, J. S. Hull, R. Abiad, T. Rodriguez-Bell, T. Magoncelli, P. N. Jelinsky, W. Donakowski, and K. E. Kromer, "Performance of the double delay line microchannel plate detectors for the Far Ultraviolet Spectroscopic Explorer," Proc. SPIE **3114**, 283–294 (1997).
18. J. B. McPhate, O. H. W. Siegmund, G. A. Gaines, J. V. Vallerga, and J. S. Hull, "Cosmic origins spectograph FUV detector," Proc. SPIE **4137**, 25–33 (2000).
19. O. Y. Ziyuan, L. Chunlai, and Z. Yongliao, "The scientific object of the first phase project of Chinese lunar exploration," Spacecraft Eng. **14**, 1–5 (2005).
20. C. Bo and H. Fei, "Optical design of moon-based earth's plasmaspheric extreme ultraviolet imager," Opt. Precis. Eng. **19**(9), 2057–2062 (2011).
21. H. O. Anger, "Survey of radioisotope cameras," Instr. Soc. Am. Trans. **5**, 311–344 (1966).
22. C. Martin, P. Jelinsky, M. Lampton, and R. F. Malina, "Wedge-and-strip anodes for centroid-finding position-sensitive photon and particle detectors," Rev. Sci. Instrum. **52**(7), 1067–1074 (1981).
23. J. S. Lapington, "A comparison of readout techniques for high-resolution imaging with microchannel plate detectors," Nucl. Instrum. Methods. A **525**(1-2), 361–365 (2004).
24. J. S. Lapington and H. E. Schwarz, "The design and manufacture of Wedge and Strip Anodes," IEEE Trans. Nucl. Sci. **33**(1), 288–292 (1986).
25. M. L. Edgar, R. Kessel, J. S. Lapington, and D. M. Walton, "Spatial charge cloud distribution of microchannel plates," Rev. Sci. Instrum. **60**(12), 3673–3680 (1989).
26. C. H. Mosher, "Pseudo-Gassian transfer functions with superlative baseline recovery," IEEE Trans. Nucl. Sci. **23**(1), 226–228 (1976).
27. A. S. Tremsin and O. H. W. Siegmund, "Spatial distribution of electron cloud footprints from microchannel plates: Measurements and modeling," Rev. Sci. Instrum. **70**(8), 3282–3288 (1999).
28. A. Smith, R. Kessel, J. S. Lapington, and D. M. Walton, "Modulation effects in wedge and strip anodes," Rev. Sci. Instrum. **60**(11), 3509–3518 (1989).
29. O. Jagutzki, J. S. Lapington, L. B. C. Worth, U. Spillman, V. Mergel, and H. Schmidt, "Position sensitive anodes for MCP read-out using induced charge measurement," Nucl. Instrum. Methods Phys. Res. A **477**(1-3), 256–261 (2002).
30. L. P. He, J. Y. Yue, S. J. Liu, and B. Chen, "Polynomical correction of photon-counting position-sensitive detector's distortion," Acta Opt. Sin. **32**(6), 0604002 (2012).

1. Introduction

In the last few decades, the fast development of the silicon based IC industry allows planar focal plane detector arrays with more pixels and lower cost. As a result, the planar focal plane detector technology has dominated the imaging market from the consumer electronic digital cameras to the space-based astronomical telescopes. However, it is because of the planar detecting surface of the imaging sensors so that the optical system design becomes rather complicated in order to eliminate optical aberrations. Normally, a number of optical lenses with spherical or aspherical surfaces are needed to correct the aberrations, which makes the optical system the most expensive part of the optical camera. Therefore, it is always a great challenge to make the whole optical imaging system more compact and cost-effective. In particular for the space-based telescope whose size is at the meter scale and the weight at a few hundreds of Kg scale, if the size and the number of the lens can be effectively reduced, the cost of the whole imaging system can be significantly cut off so that more payloads on satellite are possible. For this purpose, curved focal plane detector arrays have been proposed in that it has the advantage to achieve a good optical image with a relatively simpler optical system design [1]. To realize curved focal plane detector arrays, different strategies were

#242423 Received 5 Jun 2015; revised 1 Nov 2015; accepted 10 Nov 2015; published 17 Nov 2015

proposed [2–10]. These methods include the direct fabrication of image sensor arrays by soft-lithographic method [2,7] on curved surfaces, or by deforming the stretchable or compressible planar counterparts into their curved ones [3–6,8] or by mechanically deforming the rigid planar focal plane detector array directly [10].

So far, aforementioned curved focal plane detector arrays are mainly working on ultraviolet, visible or infrared wavebands, and only a few of curved focal plane detector arrays working at extreme ultraviolet (EUV) waveband were reported [11–18]. In this work, a curved focal plane detector array working at 30.4 nm wavelength is reported. The details of the fabrication, the characterization and the discussion about the curved focal plane EUV detector array are discussed. The developed curved focal plane EUV detector array has been equipped into the EUV camera and launched as a payload on Chang E Lander in the second phase of the Chinese lunar exploration project in 2013 [19,20]. The EUV camera is now running based on the moon to study the distribution of He^+ in Earth's plasma sphere by detecting its resonantly-scattered emission at 30.4 nm.

2. Fabrication of the MCP Based Curved Spherical Surface

In order to capture the image of the He^+ emission of the global plasma sphere effectively, the moon-based EUV camera must have a field of view 15°. To save space and weight, the optical system is designed to only have a single spherical mirror with Mo/Si multilayer coating on its surface. The central working wavelength of the optical system is 30.4 nm with a bandwidth of ± 5 nm. For the sake of eliminating the optical aberrations effectively, the focal plane of the EUV camera is designed to have a spherical surface. Therefore, a two-dimensional photon-counting imaging detector array based on a spherically curved bare microchannel plate (MCP) stack is designed. The angular resolution of the EUV camera is 0.08°. Considering the focal length of the optical system is 148 mm, the pixel resolution of the curved detector array is determined to be 0.2 mm, i.e. 2.5 lp/mm. There are 188 pixels in total in the whole 15° field of view, which means that the sensitive area of the curved detector array has have a diameter of 37.6 mm. In that the emission intensity of the He^+ Emission of the plasma sphere ranges from 0.1 R to 10 R at 30.4 nm wavelength, the sensitivity of the EUV camera should be no less than 0.11 count/s·R, and hence the background noise must be less than 1 count/s·cm^2 and the maximum global count rate should be 43 kcps. Here R is the abbreviation of 'Rayleigh', which is a unit of photon flux. Thus, the image linearity of the EUV camera is calculated to be 0.1 mm. The detector's operating temperature ranges from −15 °C to + 70 °C due to the large temperature difference from −180 °C to + 120 °C on the Moon.

The key technology to fabricate the curved focal plane EUV detector array is to make a spherical surface on MCPs. There are two ways to make a spherical surface on the MCP stack. One is to lap and polish each MCP surface to the required spherical one prior to etching and removing of the MCP core glass. This method can produce a spherical surface with an accurate radius of curvature but the gain uniformity is relatively poor due to the different length-to-diameter (L/D) ratio for each MCP in the stack. However, the position of the focal plane is quite exact due to the accuracy of the radius of curvature of the surface of the MCP. This technique has been applied to the MCPs for the soft X-ray and EUV astrophysics mission ALEXIS [11,12]. The other is to thermally slump a flat MCP surface into a required spherical one before core glass etching. For this method, the radius of curvature of the formed MCP spherical surface can't be controlled as accurate as that of the former method, but the gain and gain uniformity are better due to the same L/D ratio of each microchannel. However, the formed image on the curved MCP surface might be out of focus in some areas. This method has been applied to make the curved MCPs for the ROSAT wide field camera and the IMAGE EUV camera with a 30° field of view [11]. For our moon-based EUV camera, a new method by taking advantage of the merits of above two mentioned methods to make a MCP based curved focal plane detector array was proposed. In our method, the flat MCP with a

#242423 Received 5 Jun 2015; revised 1 Nov 2015; accepted 10 Nov 2015; published 17 Nov 2015

greater thickness than the required was first thermally slumped into a spherical surface before core glass etching, and then followed by the lapping and polishing of each MCP surface to the desired radius of curvature and thickness to ensure an accurate radius of curvature and uniform L/D ratio. By using above new method, the MCP based curved spherical surface with a L/D ratio of 80:1 for each MCP, bias angles ranging from 0° to 13°, and a radius of curvature of 150 mm were successfully fabricated. Figure 1(a) shows the formed MCP based curved surface and Fig. 1(b) shows the finished MCP curved surface.

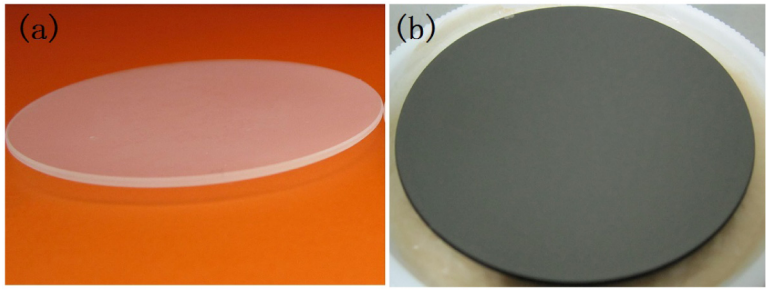

Fig. 1. Photographs of the formed MCP based curved surface (a) and the finished curved surface (b).

3. Two-dimensional Curved Focal Plane Detector Array and its characterization system

By using the above fabricated curved MCP, a novel curved focal plane detector array with an induced charge wedge-strip anode (WSA) for photon-counting imaging has successfully developed [21,22]. The detector consists of a Kovar-alumina brazed body assembly containing MCP stacks and the readout anode. The MCP stack is formed by using three 46 mm-diameter curved MCPs with one placed on the top of the other. Each MCP has an 80:1 L/D ratio and a 12 μm-diameter core. The radius of the MCP curved surface is 150 mm. The resistance for each curved MCP is about 100 MΩ. The top MCP has a 0° bias angle and the middle and the bottom MCPs have a left and right bias angles of 13° respectively. The MCP stack is circumferentially clamped into the brazed body assembly by using an annular shim and four small square springs. The MCP stacks are mounted 4 mm above the induced charge WSA, and a −200 V is applied across the MCP-to-anode gap by using a resistor mounted on the external wall of the brazed body. Figure 2 shows the exploded diagram of the curved MCP photon-counting detector with an induced charge WSA. Figure 3 shows the assembly of the curved MCP photon-counting detector and the photograph after it is mounted in the EUV camera.

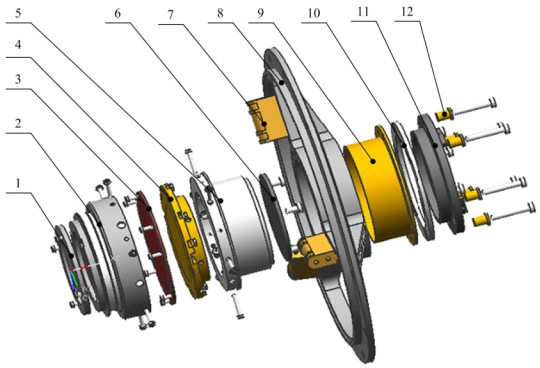

Fig. 2. An exploded diagram of the curved MCP photon-counting detector with an induced charge WSA. Where: 1. Al film filter, 2. Kovar-alumina brazed body assembly containing MCP stacks, 3. Induced charge WSA, 4. Polyimide support bracket for fixing induced charge

#242423 Received 5 Jun 2015; revised 1 Nov 2015; accepted 10 Nov 2015; published 17 Nov 2015

WSA, 5. Al support bracket, 6. Steel flange with SMA connectors, 7. Polyimide divided resistance holder, 8. Titanium alloy stand to fix detector into the EUV camera, 9. Polyimide sleeve, 10. Al pad, 11. Mounting block, 12. Polyimide insulated barrel.

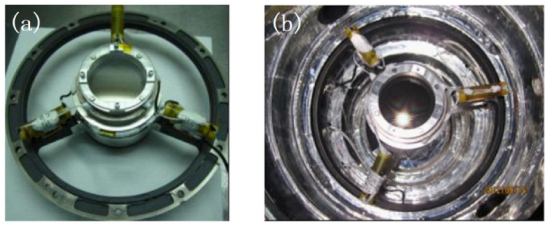

Fig. 3. Photography of the curved MCP photon-counting detector (a) and the photograph of it after mounted into the EUV camera (b).

In order to avoid the image non-linearity and distortion which results from the redistribution of the charges by secondary emission from the surface of the metal anode, an induced charge WSA is designed and used. Induced charge wedge strip anode is a kind of charge collection anode. In the induce charge wedge strip anode, there is an insulating glass layer sandwiched in between the resistive layer and the metal wedge-strip anode so that a capacitor is formed. In this case, the electrons are not directly collected by the metal wedge-strip anode, whereas the electrons ejected from the MCP stack incident onto the resistive layer and the capacitive structure allows the charge pulse is induced onto the metal wedge-strip anode. There are two advantages of induced charge wedge strip anode. One is that the image has a good linearity. The other is that the partition noise caused by the random distribution of the directly collected charge cloud can be eliminated [29]. The three-electrode WSA of the induced charge anode is designed to have a repetition period of 1.5 mm, 32 periods in total. The insulation gap in between the resistive layer and the metal wedge- strip anode is 50 μm, covering a circular area with a 48 mm diameter. The three electrodes are in the form of two combs, the wedge and strip, and the interleaved zigzag shape respectively. The strip width increases linearly across the anode area in one direction, while the wedge width increases linearly in the perpendicular direction. The other surface is coated by a Ge resistive film with a great surface resistivity. Here, "surface resistivity" means the sheet resistance of a thin film with a uniform thickness. The sheet resistance can be directly measured by using a four-point probe measurement. The sheet resistance of the Ge resistive film was measured to be about 100~800 MΩ/square at temperature ranging from + 70 °C to −15 °C. The great surface resistivity is to make sure that the time for the event charge to dissipate is far longer than that taken by the readout electronics to process the event charge. The Ge film was prepared by RF magnetron sputtering method.

The round WSA was fabricated by using a picosecond laser processing technology. Typically, the conductor is a 2 μm-thick Al film directly deposited on a 1.5 mm-thick quartz substrate, which is electrically connected to four square copper metallization electrodes. These electrodes are used to weld conducting wires to SMA connectors which are connected to front-end analog circuit. A lot of debris is found left on the edge of the insulated grooves which are formed during the picosecond laser pulse ablation process. To remove the debris, the processed metal film was washed in the ultrasonic pool full of methanol for several minutes. After cleaning and drying, the width and the depth of the grooves were measured by an atomic force microscopy. The measured results show that the groove has a depth of about 2.529 μm. Since the depth is larger than the metal film thickness, i.e. 2 μm, it means that the metal film in the groove has been completely removed. The inter-electrode capacitances between W, S and Z electrodes are 50 pF, 110 pF and 110 pF respectively. The Z electrode has a resistance of 140 Ω. Figure 4 shows the photograph of the induced charge WSA anode. The Ge film is shown in Fig. 4(a) and the metal WSA is shown in Fig. 4(b).

#242423 Received 5 Jun 2015; revised 1 Nov 2015; accepted 10 Nov 2015; published 17 Nov 2015

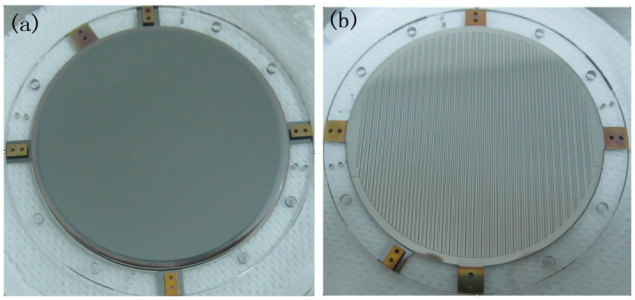

Fig. 4. Photographs of the induced charge WSA anode: (a) the Ge film surface and (b) the metal WSA surface.

4. Characterization results and discussion

In order to characterize the detector, it was placed in a vacuum chamber with a pressure of about 10^{-5} Pa to evaluate its performance by testing parameters including background rate, pulse height distribution, gain, image linearity and spatial resolution. Figure 5 shows the layout of the whole testing system. In the testing, a UV light beam was used to illuminate the USA1951 air force resolution target or pinhole array located before the detector. The detector is connected to an analog front-end and data acquisition circuit shown in Fig. 5. A negative high voltage was applied to the MCP stacks and MCP-to-anode gap via two divided resistors respectively.

The detector electronics consist of three charge-sensitive preamplifiers, amplifiers, peak holders, analog digital converters (ADCs), interface circuit and a computer, which are necessary to encode photon event data. When incident photons strike on the bare surface of the MCP, photoelectrons are excited, which are then multiplied and get accumulated onto the Ge film of the induced charge WSA. The induced charges are proportionally divided among the wedge, strip and zigzag electrodes, and then the signals are transferred to the detector electronics. Each of the three signals is amplified and converted to digital form before being sent to the computer and subsequently converted to X, Y photon positions by the use of the following formula [23–25],

$$X = \frac{2Q_S}{Q_W + Q_S + Q_Z}, Y = \frac{2Q_W}{Q_W + Q_S + Q_Z} \tag{1}$$

Where Q_W, Q_S, and Q_Z are the charge collected by the wedge, strip and Z electrode respectively. The centroids of the electron clouds accumulating on the three electrodes of WSA can be exactly represented by X, Y coordinates.

#242423 Received 5 Jun 2015; revised 1 Nov 2015; accepted 10 Nov 2015; published 17 Nov 2015

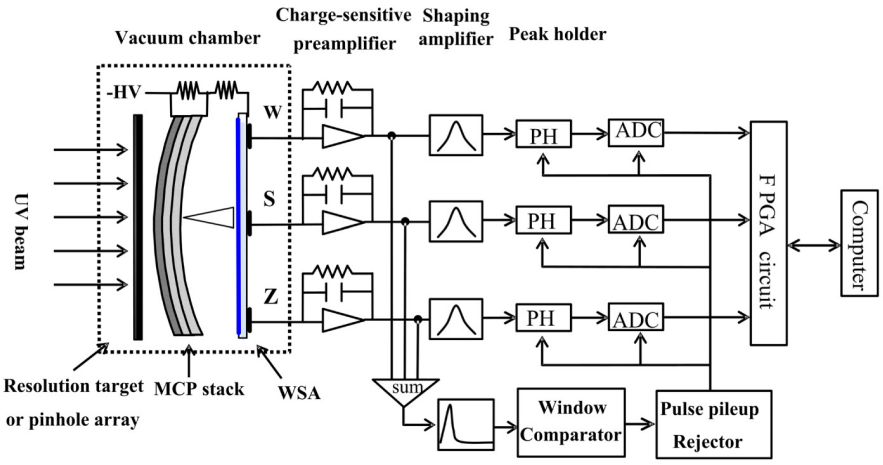

Fig. 5. Framework plot of induced charge WSA photon-counting imaging system for the testing the performance of the MCP based curved focal plane detector array.

The charge pulses from each electrode are fed into a charge-sensitive preamplifier, a shaping amplifier with 0.5 μs shaping time, a peak holder with 2 μs sample hold time, and a 12 bit A/D with 2 MHz sampling rate. The sum of three preamplifiers output pulse signals is then fed into a fast amplifier with a 40 ns shaping time. The output from the fast amplifier is considered as the input of a window comparator producing Transistor-Transistor Logic (TTL) pulses with tens of ns pulse width, then the TTL pulses are sent to a pulse pileup rejection circuit for the sake of removing all pileup pulses and generating all controlling pulses for the following ADCs, peak holders and interface circuit. The coordinate (X, Y) is calculated by the software in real-time mode according to formula (1) and the entire circuit can achieve a count rate of up to 100 kcps.

The input stage of the charge-sensitive preamplifier consists of an n-channel Junction Field Effect Transistor (JFET) (2N4416) and a low noise wide bandwidth operational amplifier (THS4031). Since the equivalent input voltage noise of JFET is 6 nV/√Hz and the equivalent input capacitance of JFET is 10 pF, therefore the resulting transconductance of the JFET is 5 mA/V. The feedback capacitance and resistance of preamplifier are 3 pF and 100 MΩ, respectively. The measured rise time and equivalent input charge noise of preamplifier are 8 ns and 230 electrons (root mean square, RMS), respectively.

The requirement for high counting rate capability dictates the use of a pulse-shaping network with a short dead time. For this reason, a Gaussian shaper is chosen in that it performs well and requires fewer stages to implement. Moreover, the Gaussian shape also offers a flatter top that is less sensitive to timing jitter and pulse shape variations when using a peak hold approach.

The semi-Gaussian shapers are implemented by using simple passive RLC networks with two stages and buffered by the pulse amplifier (THS4031) to form a 3-pole arrangement based on the method of Mosher [26]. Pole-zero compensation is done to correct the charge-sensitive preamplifier fall time. The outputs of the shapers exhibit excellent matching, symmetry, and baseline recovery without requiring circuit trims.

The peak holder is used to track shaping amplifier's input pulse and keep the maximum output pulse amplitude as a peak voltage on a hold capacitor, which has a high speed, extremely low drop rate and fast discharge time.

4.1 Gain and Pulse Height Characteristics

The pulse height distribution (PHD) of a single photon event is one of very important characteristics of the curved MCP detector. PHD is usually characterized by the ratio of the

#242423 Received 5 Jun 2015; revised 1 Nov 2015; accepted 10 Nov 2015; published 17 Nov 2015

half-width at peak (full width at half maximum: FWHM) to the peak value in PHD. Since PHD is independent on wavelength, its measurement were conducted with a uniform 253.7 nm light illumination radiating from a pen Hg lamp using a fused silica diffuser. Figure 6(a) shows the measured PHD against the electron number of each output pulse from the anode for different high voltage applied to MCP stack, the gain of MCP stack is the peak value in PHD. The FWHM of PHD and gain as a function of high voltage applied to MCP stack are shown in Fig. 6(b), the PHDs have a range of about 98%~136% for different high voltages applied to MCP stack. Specifically for a 3350 V and 3450 V MCP stack applied high voltage, the peaks at PHD correspond to a gain of about 1.86×10^7 and 2.5×10^7, respectively.

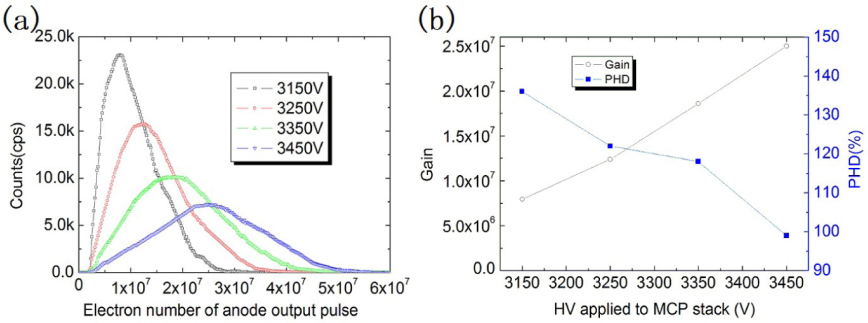

Fig. 6. MCP stack PHD for different high voltage (a) and FWHM of PHD and gain as a function of voltage (b).

4.2 Background noise

The MCP stack has an intrinsic background noise which can be induced by cosmic ray. Field emission and the natural radio activity of the glass containing the radioactive decay ^{40}K are the main source of the dark counting. Therefore, an efficient method to reduce the background rate is to use a glass without ^{40}K. For our case, a kind of glass contains no Potassium or Rubidium but Sodium or Caesium element is used. The composition of the glass is 65% SiO_2, 20.5% (PbO + Bi_2O_3), 3%(Na_2O + Cs_2O) and 11.5%(TiO_2 + Gd_2O_3 + BaO + Al_2O_3). Figure 7 shows the measured background noise of the curved MCP detector at a temperature of 72.6 °C. As can be seen, the background noise is quite uniform and the average of its fluctuation is less than 0.3 counts/s·cm^2 for a given photon number at different fixed exposure time of 2 minutes, 10 minutes and 20 minutes. Since the sensitivity of EUV camera is designed to be 0.1~0.2 counts/s·R, this requires that the background noise of the detector is less than 1 counts/s·cm2, therefore the background of the detector is sufficient for the potential measurement.

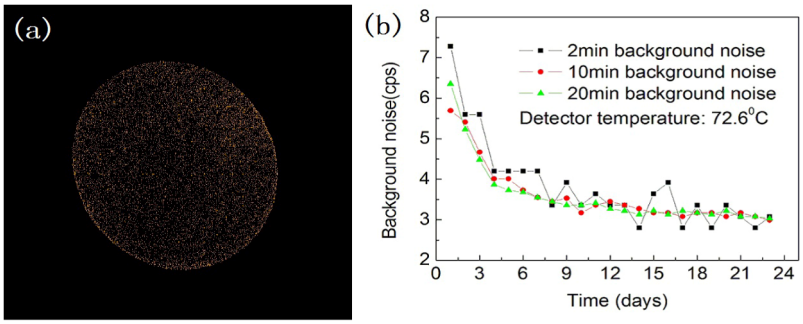

Fig. 7. A background noise image for 10 min exposure time (a) and the background noise VS time for different exposure time at a temperature of 72.6 °C (b).

#242423 Received 5 Jun 2015; revised 1 Nov 2015; accepted 10 Nov 2015; published 17 Nov 2015

4.3 Spatial resolution and image distortion

The spatial resolution is another very important characteristic for the curved MCP detector. Detectors with a metal WSA and three different curved MCP stacks were designed and manufactured during the preliminary stage of the project. These three curved MCPs have the same radius of curvature of 150 mm, the same diameter of 46 mm and the same L/D of 80:1 but with different bias angles. The bias angle of a microchannel plate is the angle between the normal of the MCP surface and the channel direction. Typical bias angles range from 5° to 15°. In our case, the bias angles for three MCPs in the MCP stack have bias angles of 0°, 13° (right bias) and 13° (left bias) from top to bottom respectively. The aim of such an arrangement on the bias angles is to avoid the ion feedback problem. As a result, the detection efficiency of a MCP for charged particles and electromagnetic radiation can be optimized by controlling the incident angle of the input event. The metal WSA anode has 44 periods and each period is 1 mm. In the interest of getting the image with high resolution and low distortion, the size of the electron cloud is optimized. It is reported that the size of the electron cloud footprint strongly depends on the MCP-anode gap and the applied voltage [27,28]. The larger electron cloud footprint will result in the larger image distortion, while the smaller electron cloud footprint will have a stronger modulation effect on the image due to the comparable size between the electron cloud and the WSA pattern period [29]. To characterize the resolution and distortion of the image formed on the detector, a USAF1951 spatial resolution target in contact with the detector was illuminated by using a spot UV light under different MCP-anode gap and applied voltage conditions. Figure 8(a) shows the image formed on the detector under the condition of 16 mm MCP-anode gap and −200 V applied voltage. In this case, the voltage applied to MCP stacks is −3450 V and the gain of MCP stack is about 2.5×10^7. As can be seen, the image is out of round and has a great distortion on the edge. Therefore, it is quite difficult to obtain a circular image by just using the image correction algorithm. Furthermore, it is clear that the image of the 2nd element of the 2nd group of USFA1951 resolution target pattern can be resolved, which means the spatial resolution in this case is 4.49 lp/mm. It is found that by changing the MCP-anode gap and the applied voltage, the distortion of the image can be improved significantly without losing the spatial resolution. As can be seen from Fig. 8(b), when the MCP-anode gap is reduced from 16 mm to 8 mm with a corresponding applied voltage of −300 V, the shape of the image becomes rounder and rounder and the distortion of the image becomes smaller and smaller. This means that a smaller MCP-anode gap is favorable for a better image. In addition, if the applied voltage to MCP-anode is increased, the distortion of the image can be improved further. However the images obtained in Fig. 8(b) still have apparent distortions, hence it is difficult to get a circular image with small distortion.

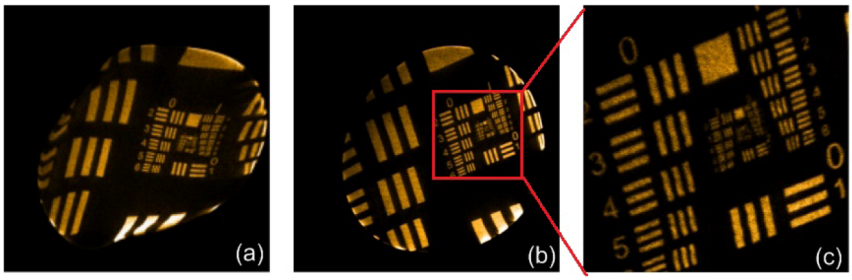

Fig. 8. The UV image of USAF1951 resolution target for metal WSA with MCP-anode gap: a) 16mm and b) 8mm, applied high voltage to MCP-anode is 200V and 300V

#242423 Received 5 Jun 2015; revised 1 Nov 2015; accepted 10 Nov 2015; published 17 Nov 2015

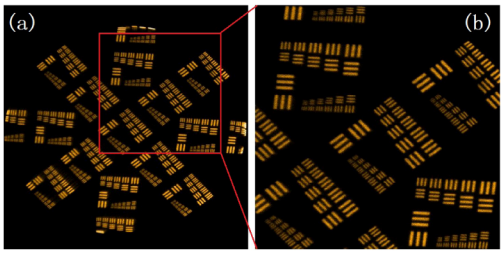

Fig. 9. The UV image of USAF1951 resolution target with 1-2 groups for induced charge WSA photon-counting imaging system at 72.6°C.

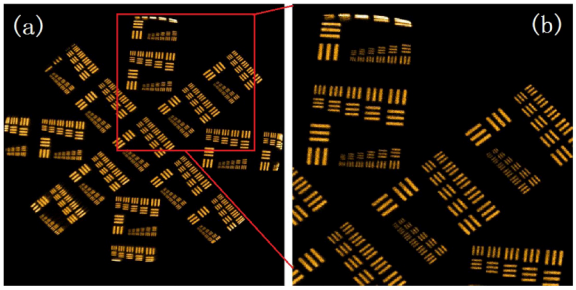

Fig. 10. The UV image of USAF1951 resolution target with 1-2 groups for induced charge WSA photon-counting imaging system at −18°C.

In order to solve the problem on image distortion produced by metal anodes, an induced charge WSA shown in Fig. 4 is made instead of the metal anode. In this case, the minimum MCP-anode gap can be reduced to about 4 mm. The active diameter of the circular anode is set to be 48 mm so that the image distortion appeared on the edge can be minimized. Figures 9 and 10 show the 1-2 group USFA1951 target images with this anode under the conditions of a 10 min exposure time and 50 kcps global count rate at the temperature of 72.6°C and −18°C, respectively. As is shown these images have a round shape and the distortion on the edge of the image is not notable. All elements in the 1-2 group of USFA1951 resolution target pattern are clearly resolvable, which means the spatial resolution is 7.13 lp/mm. In this measurement, the voltage applied to MCP stacks is −3350 V and the gain of MCP stack is about 1.86×10^7. The reason why the spatial resolution is significantly improved is due to the elimination of the partition noise which often exists in metal WSA.

4.4 Linearity of the image

The linearity of the detector was measured by placing a two-dimensional pinhole array in front of the detector illuminated by a spot UV light. The diameter of each pinhole is 50 micron and the spacing between pinholes is 2 mm in both X and Y directions. Figure 11 shows the image of the pinhole array captured by the detector. As can be seen, there is a barrel distortion on the image shown in Fig. 11(a). This kind of the image distortion can be attributed to two reasons. One is the pulse crosstalk between electrodes, and the other is the non-uniform distribution of the electric field on the edge of the anode. A good image correction can be done by employing a polynomical correction method [30] and Fig. 11 shows the images before and after the correction. The mean value for the image linearity shown in Fig. 11(b) is calculated to be about 100 μm within 90% field of view.

#242423 Received 5 Jun 2015; revised 1 Nov 2015; accepted 10 Nov 2015; published 17 Nov 2015

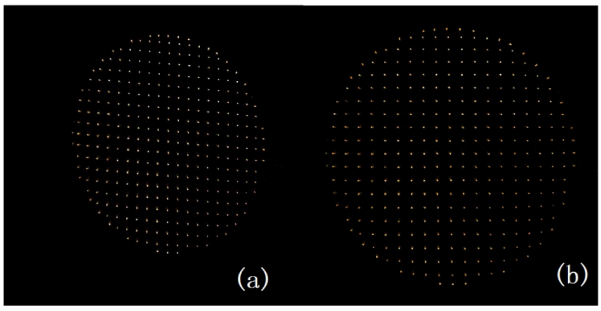

Fig. 11. Images of a pinhole array captured by the detector before (a) and after (b) the correction

4.5 Detective Quantum efficiency

Figure 12 shows the schematic diagram of the detective quantum efficiency (DQE) measurement system, which consists of a metal target laser-produced plasma (LPP) light source, a McPherson Model XCT grazing incident monochromator with 1200 G/mm grating, a vacuum sample chamber which contains a mini rotating stage, a NIST calibrated AXUV-100 photodiode and a two-channel 12 bit NI A/D card. The LPP light source is driven by a Q-switch Nd:YAG laser (Continuum 9100) operating at the single shot mode, delivering up to ~300 mJ per pulse at a wavelength of 1060 nm. The EUV radiation ranging from 10 nm~40 nm is generated from a Cu target, and is then collected and monochromatized by using a high-resolution grazing-incidence McPherson XCT monochromator in the waveband range of 5 nm~60 nm with a spectral resolution of 0.2 nm. The outputting monochromatic light beam incidents onto the bare curved MCP detector which has a 0° bias angle MCP and a metal anode, or the NIST calibrated AXUU-100, positioned on the rotating stage and connected to a common electronic system. The electronic system includes a charge-sensitive preamplifier, a shaping amplifier, a NI A/D card integrated into a PCI slot of a computer. The MCP and AXUV-100 motion is controlled by a high-resolution stepping-motor controller. The DQE in 20 nm~40 nm was measured by scanning wavelengths. The DQE versus the incident angle is achieved by rotating the MCP detector. The DQE at the wavelength λ is given by the following formula,

$$DQE(\lambda) = \frac{V_{mcp}(\lambda) \cdot A_{axuv} \cdot R_e(\lambda) \cdot h\gamma}{V_{axuv}(\lambda) \cdot A_{mcp} \cdot G_{mcp} \cdot e} \tag{2}$$

Where V_{mcp} (λ) is the amplitude of shaping amplifier output pulse for MCP detector, V_{axuv} (λ) is the amplitude of shaping amplifier output pulse for the NIST calibrated AXUV-100, A_{mcp} and A_{xuv} are amplified multiple of shaping amplifier for MCP and AXUV-100 output signal respectively, R_e(λ) is the DQE of the NIST calibrated AXUV-100, G_{mcp} is the gain of the MCP detector operating in the analog mode. It is assumed that MCP gain is only determined by the high voltage applied to the MCP. The constants in the formula are defined as follows: γ = c/λ, c = 3 × 10^8 m/s, e = 1.6 × 10^{-19} C, h = 6.626 × 10^{-34} m^2·kg/s. The DQE at 30.4 nm was measured to be 14.6% and 16.1% for 10° and 15° incident angles, respectively.

#242423 Received 5 Jun 2015; revised 1 Nov 2015; accepted 10 Nov 2015; published 17 Nov 2015

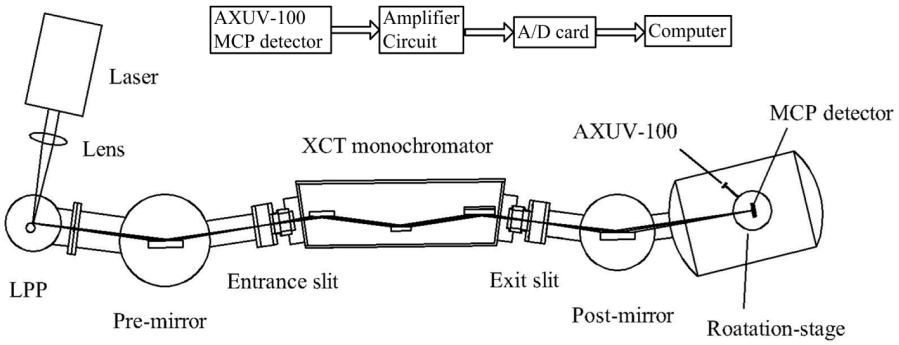

Fig. 12. Schematic diagram of detective quantum efficiency measurement system

5. Conclusions

According to the requirements of the moon-based EUV camera, a prototype of two-dimensional curved focal plane detector array for photon-counting imaging has been developed based on the curved MCP. The curved MCP was fabricated by using a new fabrication method which retains the merits of other reported methods. As a result, the fabricated curved MCP surface does not only have an accurate desired radius of curvature, but also has the same L/D ratio for each microchannel. Based on the newly fabricated MCP, the two dimensional curved focal plane detector array working at EUV wavelength was fabricated associated with the testing electronic system. The fabricated curved detector array was then characterized to have a spatial resolution of 7.13 lp/mm, a quantum efficiency of >14%, a linearity of 100 μm, a quite small background noise with a fluctuation of less than 0.3 counts/s·cm^2 and a gain of 10^7 scale. Moreover, the optimum working condition under which a distortion free image can be obtained was also explored. In summary, the developed curved focal plane EUV detector array in this work can fulfill the requirements of the moon-based EUV camera for the purpose of capturing the image of the global plasmaspheric He^+ emission.

Acknowledgments

This work is supported by the National Natural Science Foundation of China under Grant No.61475154, 61275152, 61361166004 and 61475156.

#242423 Received 5 Jun 2015; revised 1 Nov 2015; accepted 10 Nov 2015; published 17 Nov 2015